A 200 000 rpm, 2 kW Slotless Permanent Magnet Motor

Pierre-Daniel Pfister, *Student Member IEEE* and Yves Perriard, *Senior Member IEEE*

Integrated Actuators Laboratory (LAI), Ecole Polytechnique Fédérale de Lausanne (EPFL), 1015 Lausanne, Switzerland

***Abstract*—The paper presents the development of a very high speed (200 krpm, 2 kW) slotless permanent magnet motor, using an analytical model. The multiphysics analytical model allows a quick optimization process. The presented model includes the magnetic fields, the mechanical stresses in the rotor, the electromagnetic power losses, the windage power losses and the power losses in the bearings. The paper also presents the results of the measurements on a prototype that reached 200 krpm.**

***Index Terms*—Very high speed, Slotless permanent magnet motor, Multiphysics analytical modeling, Optimization.**

I. Introduction

Due to their high power density, very high speed (VHS) permanent magnet (PM) motors are increasingly demanded on the market [1]. Indeed, as the mechanical power is given by $P = T\omega$, for a given output power P at high speeds ω one needs a much lower torque T and volume than at lower speeds.

VHS motors can allow small energy conversion systems to have high efficiency. They are hence used in energy conversion systems such as gas turbines, turbochargers [2] and superchargers [3].

The domains of applications of VHS machines are very diverse: automotive industry (supercharger, electrically assisted turbocharger, fuel cell compressor), machining industry (micro-machining), home appliance industry (vacuum cleaner), medical industry (teeth cutter), and other specific applications (compressors, cryocooler, vacuum pump, gas turbines).

In a VHS motor, the different parts and materials are pushed to their thermal and mechanical limits. Indeed, as the speed is very high, high stresses appear in the rotor. The mechanical aspects need to be considered. Also, as the energy density is high, it is critical to optimize the efficiency to decrease the power losses and hence its temperature.

A traditional way to design motors is to do the optimization using each of its submodels (thermal, mechanical, electromagnetical, ...) separately, iteratively. This is called a fragmented conception. In our case, the mechanical optimum for the motor would be to reduce the rotor diameter to diminish the stress in it, but it would reduce the motor torque. The magnetic optimum would be to reduce the air gap, but it would increase the windage power losses. These two simple examples show us the necessity of having an optimization which uses the complete multiphysics model of the system.

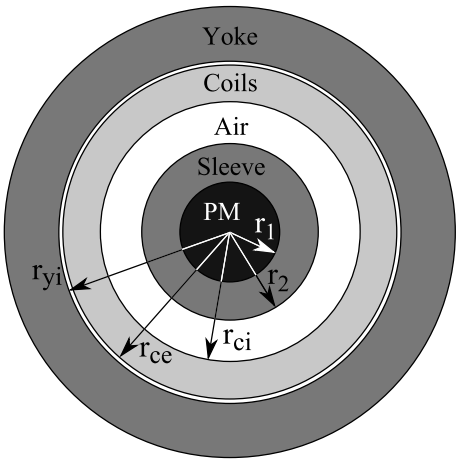

Figure 1. Motor structure

There are two different approaches for doing multiphysics systems optimization. The first one is with finite elements methods. It has the advantage that it can solve complicated structures. The disadvantage is that the computer time requirements are too long when there are different physical aspects and different parameters to optimize.

The second method is to create a fully analytical model and to do a mathematical optimization. The advantage of this method is that it is extremely fast. This method was chosen for our VHS motor development.

This article shows this innovative multiphyisics analytical optimization approach and prototype measurements.

II. The analytical model

The analytical model is applied to the motor structure shown in Fig. 1. Our geometry is: a PM at the center, a sleeve, an air gap, 3 coils and a stator yoke.

A. The torque due to magnetostatic fields

Using Xia and Zhu's article [4], the torque T produced by the interaction of one coil and the PM is calculated as presented in [5]:

$$T = \frac{2B_R J l_a r_1^{p+1} \left[\frac{r_{ce}^{p+2} - r_{ci}^{p+2}}{r_{yi}^{2p}(p+2)} + g(p, r_{ce}, r_{ci}) \right] f(\alpha_i, \theta, p)}{(1+p)\left[(1+\mu_r) + (1-\mu_r)\left(\frac{r_1}{r_{yi}}\right)^{2p} \right]} \quad (1)$$

with B_R the PM remanent field, μ_r the PM relative permeability, p the number of pole pairs, J the current density, r_1 the outer radius of the PM, r_{ci} the inner radius of the coil, r_{ce} the outer radius of the coil, r_{yi} the inner radius of the stator yoke, θ the rotor position, l_a the active length, and

$$g(p, r_{ce}, r_{ci}) = \begin{cases} \frac{r_{ce}^{-p+2} - r_{ci}^{-p+2}}{-p+2} & \text{if } p \in \mathbb{N}^* \setminus \{2\} \\ \ln\left(\frac{r_{ce}}{r_{ci}}\right) & \text{if } p = 2 \end{cases} \quad (2)$$

and

$$\begin{aligned} f(\alpha_i, \theta, p) = &\sin(p(\alpha_4 - \theta)) - \sin(p(\alpha_3 - \theta)) \\ &- (\sin(p(\alpha_2 - \theta)) - \sin(p(\alpha_1 - \theta))) \end{aligned} \quad (3)$$

with α_i $i = 1, ..., 4$ the angles which set the dimensions of one coil.

B. Mechanical stresses

The mechanical stresses (σ_r, σ_α) in the rotor are calculated using the equilibrium equation [6]:

$$\frac{\mathrm{d}\sigma_r}{\mathrm{d}r} + \frac{\sigma_r - \sigma_\alpha}{r} + F_r = 0 \quad (4)$$

with F_r the radial force density.

As we make the hypothesis of a constant speed and because of the symmetry of the problem, the strain can be expressed by:

$$\varepsilon_r = \frac{\partial u}{\partial r} \quad (5)$$

$$\varepsilon_\alpha = \frac{u}{r} \quad (6)$$

with u being the radial displacement function.

Hook's law gives the dependence of the strain ε on the stresses:

$$\varepsilon_r = \frac{1}{E}(\sigma_r - \nu\sigma_\alpha) \quad (7)$$

$$\varepsilon_\alpha = \frac{1}{E}(\sigma_\alpha - \nu\sigma_r) \quad (8)$$

with E Young's modulus and ν poisson's ratio.

In a rotating system a volume element is subject to the following force density F:

$$F = \rho\omega^2 r \quad (9)$$

with ω the anglular velocity.

Equations (7) and (8) are inverted to obtain:

$$\sigma_r = \frac{E}{1-\nu^2}(\varepsilon_r + \nu\varepsilon_\alpha) \quad (10)$$

$$\sigma_\alpha = \frac{E}{1-\nu^2}(\varepsilon_\alpha + \nu\varepsilon_r) \quad (11)$$

Using (4), (5), (6), (10) and (11) we find:

$$\frac{\mathrm{d}^2 u}{\mathrm{d}r^2} + \frac{1}{r}\frac{\mathrm{d}u}{\mathrm{d}r} - \frac{u}{r^2} = -\left(\frac{1-\nu^2}{E}\right)\rho\omega^2 r \quad (12)$$

The solution of the differential equation is:

$$u = -(1-\nu^2)\frac{\rho\omega^2 r^3}{8E} + C_1 r + \frac{C_2}{r} \quad (13)$$

with C_1 and C_2 being constants.

Two regions are defined, the sleeve (s) and the PM (m). Using (5), (6) and (13), we find for the sleeve and the PM $i = s, m$:

$$u_i = -(1-\nu_i^2)\frac{\rho_i\omega^2 r^3}{8E_i} + C_{i1} r + \frac{C_{i2}}{r} \quad (14)$$

$$\sigma_{ir} = \frac{E_i}{1-\nu_i^2}\left[\frac{-(3+\nu_i)(1-\nu_i^2)\rho_i\omega^2 r^2}{8E_i} + C_{i1}(1+\nu_i) - C_{i2}\left(\frac{1-\nu_i}{r^2}\right)\right] \quad (15)$$

$$\sigma_{i\alpha} = \frac{E_i}{1-\nu_i^2}\left[\frac{-(1+3\nu_i)(1-\nu_i^2)\rho_i\omega^2 r^2}{8E_i} + C_{i1}(1+\nu_i) + C_{i2}\left(\frac{1-\nu_i}{r^2}\right)\right] \quad (16)$$

Let r_2 the outer radius of the sleeve. We have the following conditions at the boundaries:

$$\sigma_{mr}(r=0) = \sigma_{m\alpha}(r=0) \quad (17)$$

$$\sigma_{mr}(r=r_1) = \sigma_{sr}(r=r_1) \quad (18)$$

$$\sigma_{sr}(r=r_2) = 0 \quad (19)$$

$$u_m(r=0) = 0 \quad (20)$$

$$u_m(r=r_1) = u_s(r=r_1) \quad (21)$$

We define σ_1, the radial stress at the interface:

$$\sigma_1 = \sigma_{mr}(r=r_1) = \sigma_{sr}(r=r_1) \quad (22)$$

If there is no prestressing, at no angular velocity we have:

$$\sigma_1 = 0 \quad (23)$$

Equations (14), (15), (16) have to be finite at $r = 0$. It implies that $C_{m2} = 0$.

Using (22) and (15), we find the consant C_{m1}:

$$C_{m1} = \frac{\sigma_1\left(\frac{1-\nu_m^2}{E_m}\right) + \frac{(3+\nu_m)(1-\nu_m^2)\rho\omega^2 r_1^2}{8E_m}}{1+\nu_m} \quad (24)$$

Using (14), (15), (16) we find the stresses and the displacement function in the PM:

$$\sigma_{mr}(r) = \frac{(3+\nu_m)\rho_m\omega^2 r_1^2}{8}\left[1 - \left(\frac{r}{r_1}\right)^2\right] + \sigma_1 \quad (25)$$

$$\sigma_{m\alpha}(r) = \frac{(3+\nu_m)\rho_m\omega^2 r_1^2}{8}\left[1 - \frac{1+3\nu_m}{3+\nu_m}\left(\frac{r}{r_1}\right)^2\right] + \sigma_1 \quad (26)$$

$$u_m(r) = \frac{1-\nu_m}{8E_m}\rho\omega^2 r_1^3\left[(3+\nu_m)\left(\frac{r}{r_1}\right) - (1+\nu_m)\left(\frac{r}{r_1}\right)^3\right] + \sigma_1\left(\frac{1-\nu_m}{E_m}\right)r \quad (27)$$

Equations (15), (19) and (22) define C_{s1} and C_{s2}. Knowing these constants and using (15) and (16) we find the stresses

in the sleeve:

$$\sigma_{sr}(r) = \frac{3+\nu_s}{8}\rho_s\omega^2 r_2^2\left[\left(\frac{r_1}{r_2}\right)^2 + 1 - \left(\frac{r}{r_2}\right)^2 - \left(\frac{r_1}{r}\right)^2\right] + \sigma_1\left(\frac{r_1}{r}\right)^2\frac{r_2^2-r^2}{r_2^2-r_1^2} \quad (28)$$

$$\sigma_{s\alpha}(r) = \frac{3+\nu_s}{8}\rho_s\omega^2 r_2^2\left[\left(\frac{r_1}{r_2}\right)^2 + 1 + \left(\frac{r_1}{r}\right)^2 - \frac{1+3\nu_s}{3+\nu_s}\left(\frac{r}{r_2}\right)^2\right] + \sigma_1\left(\frac{r_1}{r}\right)^2\frac{r_2^2+r^2}{r_1^2-r_2^2} \quad (29)$$

We need to calculate the contact stress σ_1 at the interface. We do that in two steps: first we calculate the stress in a no speed case and then we add the effect of the speed.

Let's first consider the case where the speed is equal to zero. The PM is fragile. In order that it does not break at high speeds, it is prestressed in the sleeve. We define the mechanical interference e to be the sum of the contraction of the magnets outer radius ($|u_m^0|$), and the expansion of the sleeves inner radius ($|u_s^0|$):

$$e = |u_s^0| + |u_m^0| \quad (30)$$

To calculate u_s^0 we consider first the sleeve without PM and calculate the displacement as a function of the stress at the interface. We use (15) with the following boundary conditions:

$$\sigma_{sr}(r_1) = \sigma_1 \quad (31)$$
$$\sigma_{sr}(r_2) = 0 \quad (32)$$

It defines the values of the two constants that we use in (14). We obtain:

$$u_s^0 = -\frac{\sigma_1 r_1}{E_s(r_2^2-r_1^2)}((1-\nu_s)r_1^2 + (1+\nu_s)r_2^2) \quad (33)$$

To calculate u_m^0 we consider the PM without sleeve. We use (15) with the following boundary conditions:

$$\sigma_{mr}(0) = \text{finite} \quad (34)$$
$$\sigma_{mr}(r_1) = \sigma_1 \quad (35)$$

It defines the two constants that we use in (14). We obtain:

$$u_m^0 = \frac{\sigma_1(1-\nu_m)r_1}{E_m} \quad (36)$$

From (30), (33) and (36) we can define σ_1:

$$\sigma_1 = -\frac{e}{r_1\left(\frac{1}{E_s}\left(\frac{r_2^2+r_1^2}{r_2^2-r_1^2}+\nu_s\right)+\frac{1-\nu_m}{E_m}\right)} \quad (37)$$

The second step is as follows: the calculation of interference e needs to take into account the effect of the speed. We calculate $u_m^\omega(r_1)$ and $u_s^\omega(r_1)$ as if there was no contact between the PM and the sleeve, no pressure, but with a given ω.

For the calculation of u_m^ω, we use the following boundary conditions:

$$u_m^\omega(0) = 0 \quad (38)$$
$$\sigma_{mr}(r_1) = 0 \quad (39)$$

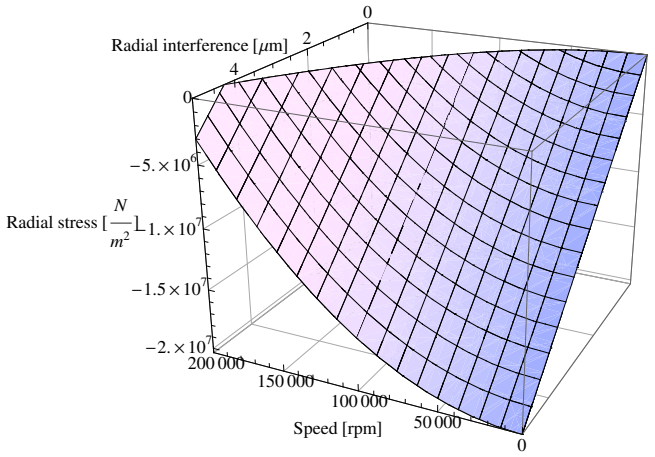

Figure 2. Radial stress at the interface between the PM and the sleeve as a function of the speed and the radial interference.

and we obtain:

$$u_m^\omega = \frac{1-\nu_m}{4E_m}\rho_m\omega^2 r_1^3 \quad (40)$$

For the calculation of u_s^ω we use the boundary conditions:

$$\sigma_{sr}(r_1) = 0 \quad (41)$$
$$\sigma_{sr}(r_2) = 0 \quad (42)$$

and we obtain:

$$u_s^\omega = \frac{(3+\nu_s)(1-\nu_s)}{8E_s}\rho_s\omega^2 r_2^2 r_1\left(\frac{2+\nu_s}{1-\nu_s} - \frac{4+\nu_s}{3+\nu_s}\left(\frac{r_1}{r_2}\right)^2\right) \quad (43)$$

Now e is modeled the following way:

$$e = u_m^\omega - u_s^\omega + e_0 + r_1(c_m - c_s)(T_r - 20\ \ ^\circ\text{C}) \quad (44)$$

with e_0 the interference between the PM and the sleeve at no speed and 20°C, c_m and c_s the dilatation coefficients of the PM and the sleeve, T_r the rotor temperature given in °C.

Using the following values:

ν_s	=	0.32	ν_m	=	0.3
ρ_s	=	4.42×10^3 $\frac{\text{kg}}{\text{m}^3}$	ρ_m	=	7.7×10^3 $\frac{\text{kg}}{\text{m}^3}$
E_s	=	116×10^9 $\frac{\text{N}}{\text{m}^2}$	E_m	=	150×10^9 $\frac{\text{N}}{\text{m}^2}$
c_s	=	$8.6\ 10^{-6}$ $^\circ\text{C}^{-1}$	c_m	=	$5\ 10^{-6}$ $^\circ\text{C}^{-1}$
r_1	=	6.244×10^{-3} m	r_2	=	8.24×10^{-3} m
T_r	=	20 °C			

we obtain the results shown in Fig. 2.

The limiting factors are the radial stress at the center of the PM, the tangential stress at the inner side of the sleeve at high speeds, and the radial stress at the interface. A negative radial stress σ_1 at the interface ensures that there is contact between the PM and the sleeve. Fig. 2 represents feasible designs according to this last limiting factor.

C. Thermal model

The steady state temperature T is calculated using the heat diffusion equation [7]:

$$k\nabla^2 T + \dot{q} = \rho c_p \frac{\partial T}{\partial t} \tag{45}$$

with k the thermal conductivity, ρ the material density, $\dot{q}$ the rate at which thermal energy is generated per unit of volume and c_p the specific heat.

Because of the 3D thermal interactions in the motor, and because of the air movements in the air gap, this 2D thermal model is not consistent with the reality. It is used to give us indications and not to constraint the model. Further investigations in the thermal modeling need to be done.

As the motor is designed by minimizing the total power losses, the thermal aspect is indirectly taken into account.

D. Electromagnetic power losses

Joule power losses density p_{cop} in the coils is calculated as:

$$p_{cop} = \rho_c J^2 \tag{46}$$

with ρ_c the resistivity and J the current density.

The stator iron power losses P_{iron} are assumed to be generated only by the PM. Their density p_{iron} is calculated approximately using Steinmetz equation:

$$p_{iron} = c_1 f^{c_2} \hat{B}^{c_3} \tag{47}$$

with c_i, $i = 1, 2, 3$ being empirical coefficients, $\hat{B}$ the maximum magnetic field and f the frequency. The same empirical approach used in [8] for the hysteresis power losses is used here for the iron power losses.

The eddy current and hysteresis power losses in the PM are neglected. The eddy currents in the sleeve and in the coils are also neglected.

E. Windage power losses

The article from Vrancik [9] indicates us that the windage power losses P_w are calculated as:

$$P_w = \pi C_d l r_2^4 \omega^3 \rho_{air} \tag{48}$$

with l the length considered, ω the angular velocity and ρ_{air} the air density. The skin friction coefficient C_d is calculated using an empirical formula:

$$\frac{1}{\sqrt{C_d}} = 2.04 + 1.768 \ln(Re\sqrt{C_d}) \tag{49}$$

with Re the Reynolds number:

$$Re = \frac{r_2(r_{ci} - r_2)\omega}{\nu} \tag{50}$$

with ν the kinematic viscosity.

Fig. 3 shows the windage power losses given by this model for a sleeve outer radius of 8.24 mm.

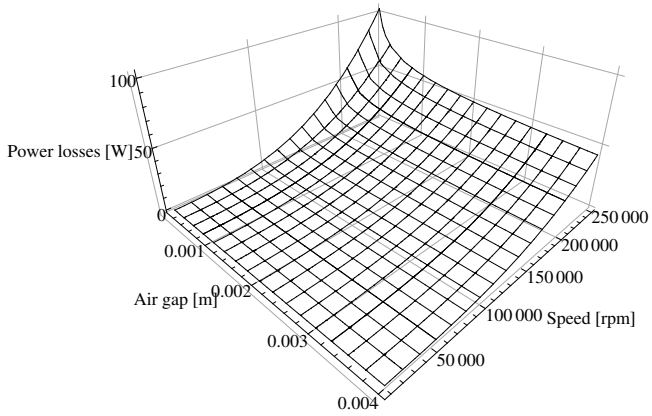

Figure 3. Windage power losses in an air gap cylinder of 34 mm of height as a function of speed and air gap thickness, for a sleeve outer radius of 8.24 mm.

Table I
MEASURED PARAMETERS OF THE BALL BEARINGS TORQUE MODEL.

Preload	17 mNm	35 mNm
c_4	1.17×10^{-6} mNm	6.12×10^{-6} mNm
c_5	2.15	1.97

F. Mechanical power losses in the bearings

The power losses in the bearings $P_{bearings}$ [10] can be estimated by:

$$P_{bearings} = c_4 \omega^{c_5} \tag{51}$$

with c_4 and c_5 be two empirical constants.

In our case, ceramic ball bearing are used. To define this model, an experimental setup was designed [11].

The measurements are fitted to the given model, as shown in Fig. 4. The friction torque of the ball bearings is dependent on the speed and on the preload.

The results are shown in Tab. I.

III. MODEL OPTIMIZATION

A. Optimization procedure

The analytical model contains more than 140 equations and 190 variables. The system has 13 degrees of freedom.

Two commercial software are used for the optimization: *Pro@Design* [12] and *Mathematica*. *Pro@Design* includes different optimization algorithms. Some are based on a sequential quadratic programming (SQP) solver using the partial derivatives and penalty functions. One parameter is chosen to be the objective function and all the others are fixed, constrained in intervals or free. *Mathematica* also includes many optimization algorithms. A code in *Mathematica* was written to handle models with large number of parameters.

B. Pareto frontiers

The suggested method for designing VHS motors allows studying Pareto frontiers.

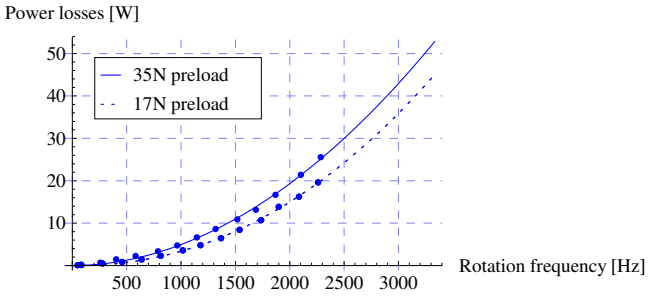

Figure 4. Friction power losses as a function of speed of a pair of ball bearings, for two different preloads. The points represent the measurements, and the curves represent the model.

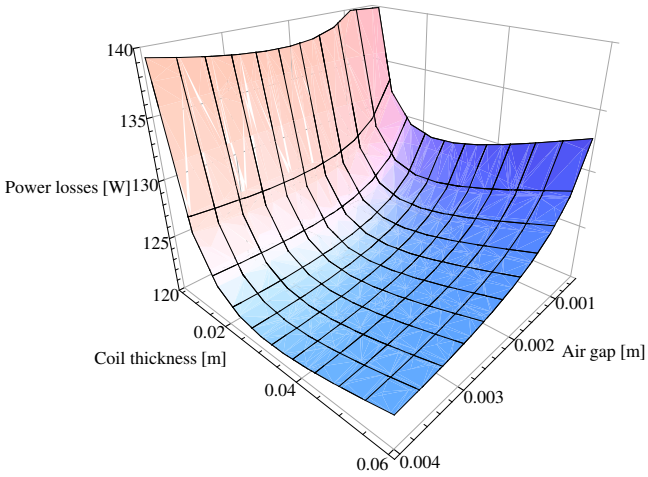

Figure 5. The Pareto frontier of the power losses, the coils thickness and the air gap.

The Pareto frontier defines optimal parameters sets. It the boundary between the feasible parameters sets and the parameters sets which are not feasible. For example in Fig. 5, the point of the surface represents the design with the lower possible power losses for a given air gap and coil thickness. Below the surface, there is no feasible design. Above the surface, the designs are not optimal.

The Figs 5 and 6 are realized by doing 100 optimizations for each figures. Nevertheless, the advantage of the purely analytical method is that it is extremely fast. It took less than 21 s for the calculation of the 100 optimizations of Fig. 6.

C. Optimization

Because of the mechanical natural frequencies, the active length of the motor was constrained to be smaller or equal to 30 mm. The prototype specifications are:

Active length of the motor (l_a)	$\leq$30	mm
PM remanence (B_R)	1.18	T
Number of phases	3	
Mechanical power	2	kW
Speed	200	krpm

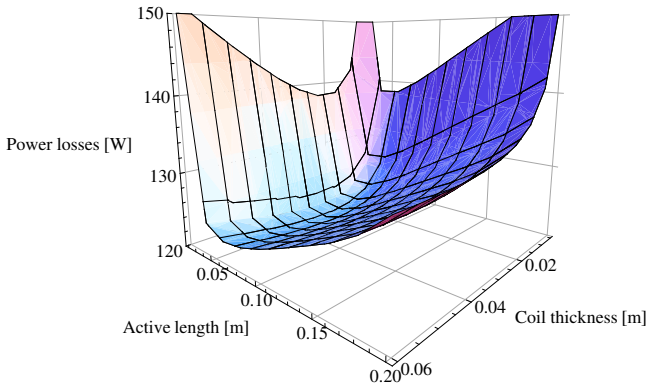

Figure 6. The Pareto frontier of the power losses, the coils thickness and the active length.

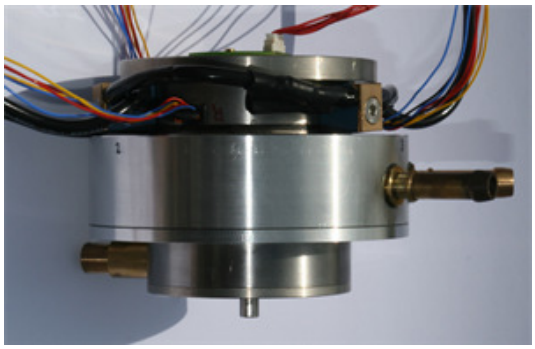

Figure 7. VHS prototype.

The design resulted from the optimization of the analytical model and some construction constraints is:

Active length of the motor	30	mm
Outer radius of the PM	6.244	mm
Outer radius of the sleeve	8.24	mm
Outer radius of the coils	16.8	mm
Air gap	1.36	mm
Number of pole pairs	1	
Phase current amplitude (sin wave)	31.14	A
Efficiency	93.7	%
Bearings power losses	53	W
Joule power losses	38	W
Air gap power losses	28	W
Iron power losses	15	W

IV. Prototype and Measurements

A prototype designed using this analytical model is shown in Fig. 7.

Fig. 8 shows the measurement of the electrical input power of the power bridge and the mechanical output power of the prototype. The maximum output power measured is 1.7 kW at 150 krpm. At this speed, the efficiency overcome 80% and the power losses are 500 W. Below 150 krpm, the prototype was limited by the current provided by the electronics; above, it was limited by the voltage. The limitation for the production

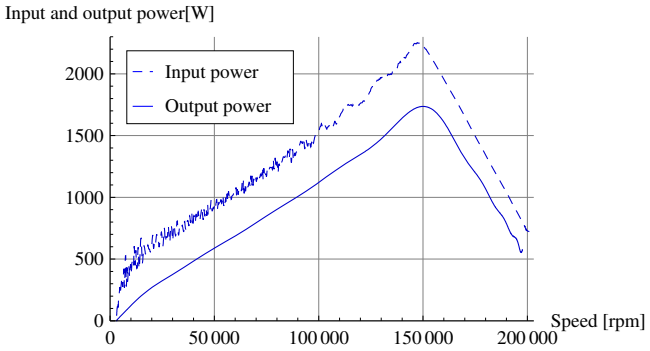

Figure 8. Electrical input power of the power bridge and the mechanical output power of the prototype.

of higher powers is the electronics. With this electronics, it takes 382 ms to accelerate the motor from 0 to 200 krpm. The measurement method is shown in [11].

V. Discussion and conclusion

The comparison of the two software used for the optimization showed that:

1) *Pro@Design* is easier to use, has more capabilities with discrete variables and is more convenient with the debugging process of the model.
2) *Mathematica* gives to the user the possibility to create tools and link them with the optimization process (mathematical language translation, advanced representation functions, other optimization algorithms, ...).
3) The same results were obtained with the two programs.

The optimization process showed in our case that:

1) It is very fast: it takes only a few seconds to find the optimum.
2) With the given restriction on the active length a 1 pole pair motor is more efficient than a 2 pole pairs.

The measurements showed that the power losses are higher than the predicted one. But the model does not include the power losses due to the power supply in the motor (except copper power losses), nor the power losses in the power supply. To improve the model, we need to consider:

1) The eddy currents power losses in the rotor produced by the field created by the coils.
2) The eddy currents power losses in the coils.
3) The iron power losses in the stator yoke due to the field created by the coils.

The construction phase showed that they are mechanical limitations that were not foreseen with the equations. In fact, the construction gave constraints on the model variables.

We are working on the electronics to be able to reach higher powers with our prototype.

VI. Acknowledgment

The authors want to thank *Moving Magnet Technologies SA* and *Sonceboz SA* for their support. They also want to thank B. Reudet for his great help in the prototyping process.

References

[1] M. Rahman, A. Chiba, and T. Fukao, "Super high speed electrical machines - summary," *2004. IEEE Power Engineering Society General Meeting*, pp. 1272–1275, 2004.

[2] Y. Yamashita, S. Ibaraki, and H. Ogita, "Development of electrically assisted turbocharger for diesel engine," in *8th International Conference on Turbochargers and Turbocharging*. Woodhead Publishing Ltd., Cambridge, CB1 6AH, United Kingdom, 2006, pp. 147–155.

[3] T. Noguchi, Y. Takata, Y. Yamashita, and S. Ibaraki, "160,000-r/min, 2.7-kw electric drive of supercharger for automobiles," in *Power Electronics and Drives Systems, 2005. PEDS 2005. International Conference on*, vol. 2, Nov. 2005, pp. 1380–1385.

[4] Z. Xia, Z. Zhu, and D. Howe, "Analytical magnetic field analysis of halbach magnetized permanent-magnet machines," *IEEE Transactions on Magnetics*, vol. 40, pp. 1864–1872, 2004.

[5] P.-D. Pfister and Y. Perriard, "Design procedure for a very high speed slotless permanent magnet motor," in *ELECTRIMACS 2008, 9th International Conference on Modeling and Simulation of Electric Machines, Converters and Systems*, 2008.

[6] A. Bazergui, T. Bui-Quoc, A. Biron, G. McIntyre, and C. Laberge, *Résistance des matériaux, troisième édition*. Presses internationales polytechniques, 2002.

[7] F. Incropera and D. DeWitt, *Fundamentals of heat and mass transfer, fourth edition*. New York: John Wiley & Sons, 1996.

[8] P.-D. Pfister, C. Koechli, M. Markovic, and Y. Perriard, "Analysis of hysteresis losses in synchronous permanent magnet motors," in *Electromagnetic Field Computation, 2006 12th Biennial IEEE Conference on*, 2006, p. 144.

[9] J. Vrancik, "Prediction of Windage Power Loss in Alternators," NASA, Tech. Rep., 1968.

[10] K. Tanimoto, K. Kajihara, and K. Yanai, "Hybrid ceramic ball bearings for turbochargers." *SAE Transactions: Journal of Materials & Manufacturing*, vol. 109, pp. 763–775, 2000.

[11] P.-D. Pfister and Y. Perriard, "Torque measurement methods for very high speed synchronous motors," in *Proceedings of the 18th international conference on electrical machines, ICEM 2008, Vilamoura , Portugal*, september 2008.

[12] "Pro@design optimization software." [Online]. Available: http://www.designprocessing.com/